Macromolecules
COMMUNICATION TO THE EDITOR

DOI: 10.1021/ma101056r

Liquid Crystalline Orientation of Rod Blocks within Lamellar Nanostructures from Rod−Coil Diblock Copolymers

Bradley D. Olsen,[†,‡] Xun Gu,[†] Alexander Hexemer,[§] Eliot Gann,[§] and Rachel A. Segalman*[,†,‡]

[†]*Department of Chemical Engineering,* [‡]*Materials Science Division, Lawrence Berkeley Laboratory, and* [§]*Advanced Light Source, Lawrence Berkeley Laboratory, University of California Berkeley, Berkeley, California 94720*

Received May 12, 2010
Revised Manuscript Received July 2, 2010

Rod−coil block copolymers have attracted a great deal of recent interest as tools for the nanostructured assembly of functional organic electronics[1,2] and biomaterials.[3,4] However, the thermodynamics of self-assembly in these systems is significantly altered from that of well-characterized coil−coil block copolymers[5,6] due to the difference in chain topology and the liquid crystalline interactions between rod blocks.[7] As a result, rod−coil block copolymers form a number of phases, some of which are not observed in coil−coil materials, including wavy lamellar,[8] zigzag,[8] arrowhead,[8] lamellar,[9,10] perforated lamellar,[10−12] hexagonal strip,[9,13,14] and puck phases.[10,13−15]

Recently, a great deal of progress has been made in understanding the equilibrium phase behavior of rod−coil systems. Lee and co-workers have extensively studied a set of systems based on short mesogenic rods and a variety of oligomeric coils, illustrating transitions between microphase-separated, liquid crystalline, and fully disordered states and mapping out the phase diagram in great detail.[9,16] Tennetti et al. have shown the effect of changing molecular weight on the type of microphase structure formed by rod−coils using a system based on mesogen jacketed liquid crystalline polymers (MJLCPs),[12] and several other groups have demonstrated well-ordered microphase structures incorporating semiconducting rods.[17,18] Our group has developed one of the few polymeric weakly segregated rod−coil systems based on poly(diethylhexyloxyphenylenevinylene-*b*-isoprene) (PPV-*b*-PI) diblock copolymers, the synthesis of which was described previously.[19] The chemical structure of this polymer is illustrated in Scheme 1. This system has demonstrated reversible transitions between lamellar, hexagonal, nematic, and isotropic phases,[19] and measurements of the Flory−Huggins interaction parameter and the Maier−Saupe parameter of rod−rod interaction have allowed a universal phase diagram to be prepared.[20] It has also been recently demonstrated that the ratio of Flory−Huggins to Maier−Saupe interaction parameters may also play a strong role.[21]

The previously reported phase behavior studies are limited in their ability to identify the liquid crystalline orientation within the ordered structures. Determining rod orientation within the block copolymer nanostructures is critically important to controlling orientation-dependent charge transport properties in organic electronic devices.[22,23] Generally, the rod orientation relative to the block copolymer interface has been inferred based upon the scaling of the domain spacing or the lamellar widths[19] or estimated from transmission electron microscopy (TEM) images,[24] providing indirect evidence for rod orientation that relies on assumed rod lengths and may be biased due to interfacial broadening and staining artifacts. Since many of the rod blocks are crystalline or form well-ordered liquid crystalline phases, a superior technique for identifying the rod orientation is the measurement of the rod diffraction peak orientation relative to the microphase orientation. While this can be performed using selected area electron diffraction,[8] temperature-dependent information on rod orientation can be more easily obtained from simultaneous SAXS/WAXS using aligned samples such that a single lamellar orientation dominates.

Scheme 1. PPV-*b*-PI Block Copolymer

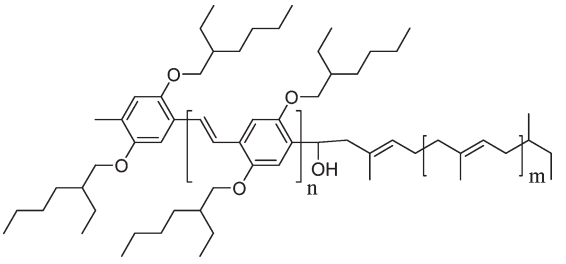

In this work, the rod orientation within macroscopically aligned samples of lamellar rod−coil block copolymers is measured to identify the liquid crystalline structure of these materials as a function of temperature, the coil to rod size ratio, and coil fraction. This allows the detailed liquid crystalline structures to be identified within the rod−coil phase diagram and provides insight into how the properties of the rod block are manifest within the block copolymer nanostructure.

Magnetic fields have been previously shown to align conjugated rod−coil block copolymers.[25] We have used this technique to prepare macroscopically aligned samples of seven weakly segregated lamellar block copolymers spanning a range of coil fractions from 0.42 to 0.87 and then identified the temperature-dependent rod orientation within the lamellar phase.

The synthesis and general phase behavior of the block copolymers used in this study have been previously reported,[19,26] and a summary of their molecular characteristics is included in Table 1, where ϕ is the coil fraction, N is the total degree of polymerization assuming a single isoprene monomer as the reference volume, and R_g/L is the ratio of the coil radius of gyration to the rod length that characterizes the polymer phase behavior.[27,28] Details on the calculation of coil fraction and molecular weight are provided elsewhere.[19] Samples for small-angle X-ray scattering (SAXS) and wide-angle X-ray scattering (WAXS) experiments were prepared and placed into a probe for magnetic field alignment (as previously described[25]) and annealed under an active flow of dry nitrogen in a 7 T magnetic field produced by a superconducting NMR magnet. Whenever possible given the temperature constraints imposed by annealing inside a cryogenically cooled magnet, samples were heated into the isotropic phase for 8 h and then annealed in the lamellar phase above the PPV crystallization temperature for 24 h. This annealing sequence was found by Tao et al. to give the highest degree of lamellar orientation, and the exact temperature used for each sample was set relative to that materials' thermodynamic transitions.[25] Limits on the safe heater temperature inside the magnet bore required samples with high liquid crystalline clearing temperatures (>160 °C, coil fractions less than 60%) to be annealed for 24 h in the nematic phase followed by 8 h in the lamellar phase. Samples were cooled to room temperature before being removed from the magnet and then annealed under nitrogen between the order-disorder transition (ODT) and the rod crystallization temperature at 0 field for

*Corresponding author. E-mail: segalman@berkeley.edu.

Published on Web 07/23/2010

Table 1. Polymer Structures and Annealing Sequences

polymer	M_n(PPV) (g/mol)	M_n(PI) (g/mol)	ϕ	N	R_g/L	ODT (°C)	LCST (°C)	annealing sequence in the magnetic field
PPVbPI-42	3500	2400	0.42	82	0.245	110	225	24 h at 160 °C, 8 h at 80 °C
PPVbPI-59	3500	4700	0.59	116	0.345	110	195	24 h at 160 °C, 8 h at 80 °C
PPVbPI-67	3400	6300	0.67	138	0.417	106	134	8 h at 150 °C, 24 h at 80 °C
PPVbPI-72	3500	8100	0.72	166	0.454	120	134	8 h at 150 °C, 24 h at 100 °C
PPVbPI-77	3400	10300	0.77	197	0.534	90	95	8 h at 120 °C, 24 h at 60 °C
PPVbPI-82	3400	13900	0.82	249	0.620	80	81	8 h at 100 °C, 24 h at 25 °C
PPVbPI-85	3400	18000	0.85	310	0.706	50	54	8 h at 100 °C, 24 h at 25 °C

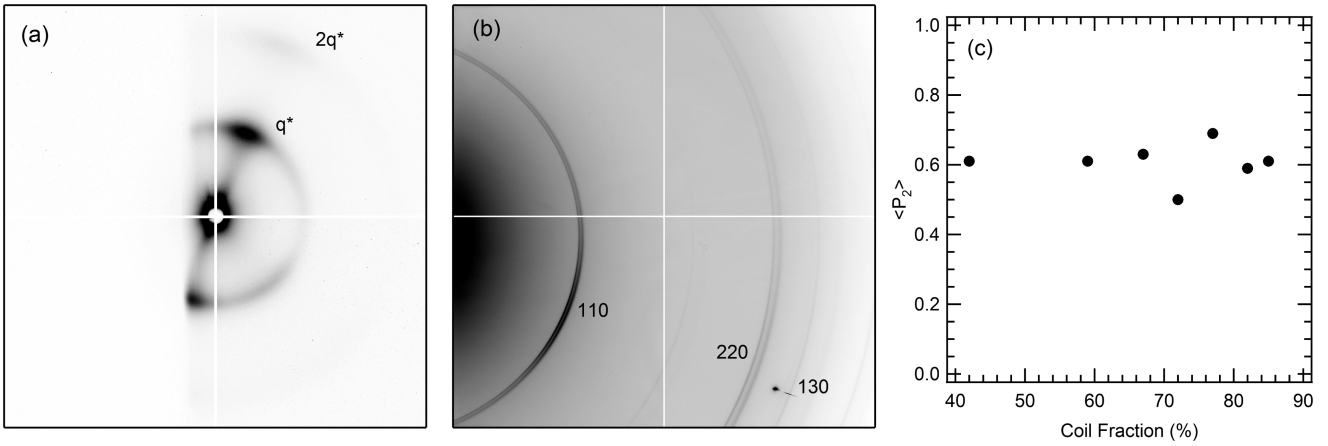

Figure 1. Small-angle X-ray scattering (SAXS, a) and wide-angle X-ray scattering (WAXS, b) images acquired simultaneously at 30 °C show the relative orientation of rod blocks to the lamellar nanostructures formed by PPVbPI-67. All oriented samples, with coil fractions ranging from 42% to 85%, showed lamellar orientational order parameters of ~0.6 (c).

an additional 24 h to minimize any anomalous effect of the magnetic field on the rod orientation relative to the lamellar microphase. The specific annealing sequence used for each sample is given in Table 1.

SAXS/WAXS experiments were performed on beamline 7.3.3 of the Advanced Light Source at Lawrence Berkeley National Lab. The beamline was configured with an X-ray energy of 10 keV and a focused spot size of ~0.5 mm diameter. Prealigned samples were heated under dry nitrogen from 30 °C to above the ODT in 5 °C increments with 10 min of thermal equilibration time allowed before data collection for 30−60 s at each temperature.

A high degree of ordering was achieved after the thermal annealing sequence for all polymers, as shown in Figure 1. SAXS patterns (Figure 1a) showed characteristically sharp peaks indicative of a high degree of lamellar orientation. The shadow of the WAXS detector obscures a portion of the SAXS pattern; however, greater than 180° of angular data is still available. Order is quantified via an orientational order parameter assuming 2-fold symmetry:

$$\langle P_2 \rangle = \frac{3\langle \cos^2 \phi \rangle - 1}{2}; \quad \langle \cos^2 \phi \rangle = \frac{\int_0^{2\pi} I(\phi) \cos^2 \phi |\sin \phi| \, d\phi}{\int_0^{2\pi} I(\phi) |\sin \phi| \, d\phi}$$

The orientational order parameter for all coil fractions was ~0.6 (Figure 1c), somewhat lower than that previously reported for a 70% coil PPV-*b*-PI. This lower degree of ordering is likely due to the secondary anneal after the sample was removed from the magnetic field. Peaks in the WAXS patterns are broader than the peaks in the SAXS patterns (Figure 1b), as previously reported; however, the WAXS still shows sufficient alignment to identify the 110 scattering peak.[29]

Heating the samples from 30 °C to above the ODT results in a disappearance of lamellar scattering as the ODT is approached, as shown in Figure 2. Below the PPV crystallization temperature, the WAXS peak intensity decreases slightly with increasing temperature and then increases sharply at the PPV melting temperature, 60 °C. In addition to the intense scattering around 35° from the aligned rods, there is also a significant contribution to the 110 reflection at other angles. The intensity of this scattering follows the same trend as the peak from the aligned rods, creating an overall shift in the WAXS scattering intensity with temperature. The SAXS peak intensity increases from 30 to 40 °C, decreases again from 40 to 50 °C, and then shows a moderate increase at 60 °C upon PPV melting. Above the melting transition, both the SAXS and WAXS peaks decrease monotonically in intensity until the ODT is reached. While these qualitative trends are reversible if the sample is not heated close to the ODT, the thermal history effects governing crystallization of the PPV rods within the lamellar nanodomains were not explored. Heating above the ODT results in an irreversible loss of orientational order.

ODTs for all the oriented polymers are similar to those determined in polycrystalline samples[19,26] within experimental error. Figure 2 clearly shows that the disordering process is marked by a decrease in peak intensity but not a broadening of the peak. This indicates that strong orientational order is preserved throughout the annealing sequence. The peaks are nearly symmetric, with the slight asymmetry most likely due to shearing caused by handling of the soft samples during loading and unloading.

The sharp increase in the WAXS peak intensity and small increase in the SAXS peak intensity suggest that the lamellar and PPV rod packing are frustrated on cooling below the PPV crystallization temperature; melting the crystals relieves this frustration and results in an improvement in ordering. Consistent with this hypothesis, an unexpected peak splitting in the WAXS peaks is also observed below the DEH−PPV melting temperature. This splitting is most clearly observed in the 110 and 220 WAXS peaks (Figure 1) and is 0.1 nm^{-1} for the 110 peak. Peak splitting has not been previously observed in any unaligned PPV-*b*-PI samples, including DEH−PPV blends,[19,26,27,30] but it is observed in all oriented samples with coil fractions of <77%. Polymers with higher PI fractions have relatively weak PPV

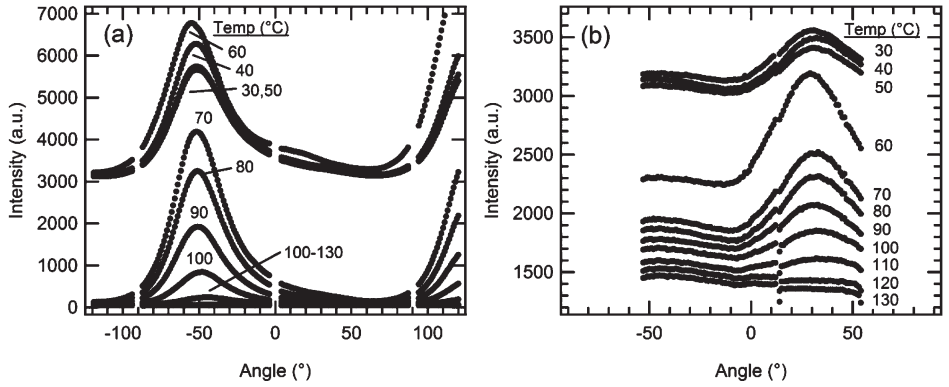

Figure 2. SAXS/WAXS radial curves as a function of temperature show a jump in scattering intensity at the DEH−PPV melting transition (60 °C) followed by a continuous drop in intensity as the ODT is approached for PPVbPI-67. SAXS data are shown in (a), while WAXS data are illustrated in (b). The ODT of this polymer is 106 °C. SAXS curves from 30 to 60 °C in (a) are offset by 3000 intensity units, and WAXS curves from 30 to 50 °C in (b) are offset by 2000 intensity units for clarity.

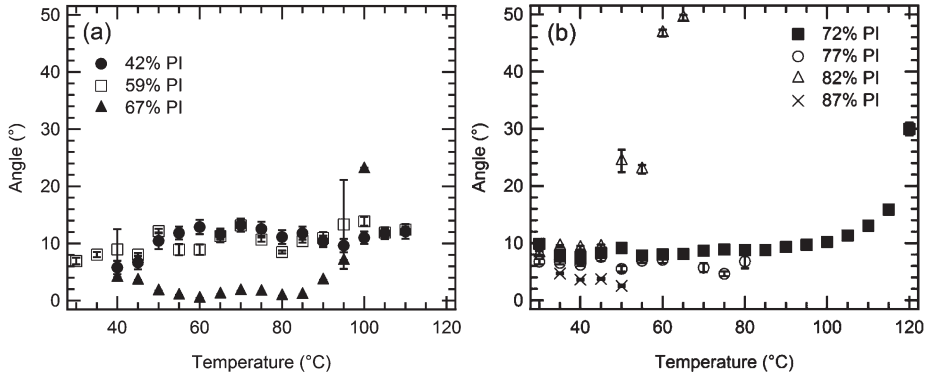

Figure 3. Relative angle between the lamellar normal and the rod director remains relatively constant between 5° and 10° for coil fractions from 42% to 85% and temperatures up to the ODT for PPV-*b*-PI block copolymers. This suggests that all these materials form lamellar phases with rods oriented nearly perpendicular to the lamellae and that orientation of the rod block is governed primarily by the crystalline or liquid crystalline packing nearly identical to that observed in the rod homopolymers.

crystallinity, so frustration is unlikely to be significant at these coil fractions.

The rod blocks of PPV-*b*-PI are oriented nearly perpendicular to the lamellar interface, and surprisingly, alignment within the lamellar nanostructures shows relatively little dependence on temperature or coil fraction. For all seven polymers, the low temperature rod tilt is 5°−10° off of the lamellar normal, and for polymers with coil fractions less than or equal to 77% this tilt persists through the DEH−PPV melting transition. This suggests that the polymers are in a smectic C phase with a very slight rod tilt, consistent with determinations of nearly perpendicular rod orientation in thin films[29] and in bulk lamellar samples based on domain spacing scaling.[27]

The weak dependence of rod orientation on temperature for all coil fractions contrasts with theoretical predictions, which suggest that heating below the ODT may result in a smectic C to smectic A transition (decrease in rod tilt) and that rod tilt should be lower at low coil fractions than at high coil fractions.[28,31,32] Our system shows small rod tilts across the entire range of coil fractions and temperatures, and if anything the rod tilt increases near the ODT. We suggest that the PPV crystalline and liquid crystalline packing, which results in a rod axis oriented along the crystalline *c*-axis or parallel to the smectic normal, is the dominant effect governing rod orientation in these systems. Furthermore, the liquid crystalline ordering of the PPV rod block within the block copolymer is nearly identical to that of the PPV homopolymer,[33] suggesting that the rod homopolymer ordering directly translates into the diblock copolymer. In order to control rod orientation and consequently the optoelectronic properties of this type of rod−coil block copolymer assembly, it appears important to control the crystalline and liquid crystalline structure of the rod homopolymer. Theories that account for more complex rod packing structures than the Maier−Saupe theory would be extremely useful in understanding this phenomenon.

Knowledge of the rod orientation and domain spacing as a function of temperature allows the molecular conformation of the block copolymers within the lamellar nanodomains to be inferred. Previous results[19,26] have shown that PPV-*b*-PI diblock copolymers show an increase in domain spacing upon increasing temperature around the ODT, with little change observed near 50% coil fraction but large increases in domain spacing observed above this coil fraction. This is in striking contrast to coil−coil diblock copolymers, where heating through the ODT results in a decrease in the characteristic size of the polymer molecule due to decreased chain stretching above the ODT. These data on rod orientation within the lamellar nanodomains clearly demonstrate that changes from smectic C to smectic A are not responsible for the large changes in domain spacing observed in the system.

Since the rod block does not reorient and is incapable of stretching, the increase in domain spacing must result from an increase in the coil size in the dimension parallel to the lamellar normal as the ODT is approached. It has been theoretically predicted that mixing Gaussian coil polymers with nematic liquid crystalline solvents results in an increase in the coil size in the direction parallel to the liquid crystalline director,[34] and large changes in coil conformation have been observed for side-chain liquid crystalline polymers in nematic solvents.[35] The analogy between the systems draws us to hypothesize that as the ODT is

approached, the increased mixing between rod and coil blocks as they become increasingly weakly segregated is responsible for extension of the coil block, leading to an unexpected increase in domain spacing around the ODT. The specific mechanism of coil elongation, however, is unclear.

Single crystalline lamellar samples of PPV-*b*-PI rod−coil block copolymers prepared by magnetic field alignment have been used to directly measure rod orientation within lamellar nanodomains. Simultaneous SAXS and WAXS measurements allow rod orientation to be quantified as the ODT is approached, showing that the rods are oriented nearly perpendicular to the lamellar interface for all coil fractions and temperatures in the lamellar phase. This suggests that crystalline and liquid crystalline packing of the rod blocks dominate rod orientation in this system and that engineering these properties will be critical for the control of optoelectronic properties in semiconducting block copolymer assemblies.

Acknowledgment. We gratefully acknowledge support from an NSF-CAREER Award. SAXS and WAXS experiments were performed at the Advanced Light Source at LBNL. B.D.O. gratefully acknowledges support from a Hertz Fellowship. We thank Dr. Yuefei Tao and Bryan McCulloch for helpful discussions.

References and Notes

(1) de Boer, B.; Stalmach, U.; van Hutten, P. F.; Melzer, C.; Krasnikov, V. V.; Hadziioannou, G. *Polymer* **2001**, *42* (21), 9097–9109.
(2) Sivula, K.; Ball, Z. T.; Watanabe, N.; Frechet, J. M. J. *Adv. Mater.* **2006**, *18* (2), 206–210.
(3) Minich, E. A.; Nowak, A. P.; Deming, T. J.; Pochan, D. J. *Polymer* **2004**, *45* (6), 1951–1957.
(4) Checot, F.; Lecommandoux, S.; Gnanou, Y.; Klok, H. A. *Angew. Chem., Int. Ed.* **2002**, *41* (8), 1339–1343.
(5) Bates, F. S.; Fredrickson, G. H. *Phys. Today* **1999**, *52* (2), 32–38.
(6) Hamley, I. W. *The Physics of Block Copolymers*; Oxford University Press: New York, 1998.
(7) Olsen, B. D.; Segalman, R. A. *Mater. Sci. Eng., R* **2008**, *62* (2), 37–66.
(8) Chen, J. T.; Thomas, E. L.; Ober, C. K.; Mao, G. P. *Science* **1996**, *273* (5273), 343–346.
(9) Lee, M.; Cho, B. K.; Kim, H.; Yoon, J. Y.; Zin, W. C. *J. Am. Chem. Soc.* **1998**, *120* (36), 9168–9179.
(10) Ryu, J. H.; Oh, N. K.; Zin, W. C.; Lee, M. *J. Am. Chem. Soc.* **2004**, *126* (11), 3551–3558.
(11) Li, C. Y.; Tenneti, K. K.; Zhang, D.; Zhang, H. L.; Wan, X. H.; Chen, E. Q.; Zhou, Q. F.; Carlos, A. O.; Igos, S.; Hsiao, B. S. *Macromolecules* **2004**, *37* (8), 2854–2860.
(12) Tenneti, K. K.; Chen, X. F.; Li, C. Y.; Tu, Y. F.; Wan, X. H.; Zhou, Q. F.; Sics, I.; Hsiao, B. S. *J. Am. Chem. Soc.* **2005**, *127* (44), 15481–15490.
(13) Radzilowski, L. H.; Stupp, S. I. *Macromolecules* **1994**, *27* (26), 7747–7753.
(14) Radzilowski, L. H.; Carragher, B. O.; Stupp, S. I. *Macromolecules* **1997**, *30* (7), 2110–2119.
(15) Cho, B. K.; Chung, Y. W.; Lee, M. *Macromolecules* **2005**, *38* (24), 10261–10265.
(16) Lee, M.; Cho, B. K.; Zin, W. C. *Chem. Rev.* **2001**, *101* (12), 3869–3892.
(17) Dai, C. A.; Yen, W. C.; Lee, Y. H.; Ho, C. C.; Su, W. F. *J. Am. Chem. Soc.* **2007**, *129* (36), 11036–11038.
(18) Sary, N.; Rubatat, L.; Brochon, C.; Hadziioannou, G.; Ruokolainen, J.; Mezzenga, R. *Macromolecules* **2007**, *40* (19), 6990–6997.
(19) Olsen, B. D.; Segalman, R. A. *Macromolecules* **2005**, *38* (24), 10127–10137.
(20) Olsen, B. D.; Shah, M.; Ganesan, V.; Segalman, R. A. *Macromolecules* **2008**, *41* (18), 6809–6817.
(21) Ho, C. C.; Lee, Y. H.; Dai, C. A.; Segalman, R. A.; Su, W. F. *Macromolecules* **2009**, *42* (12), 4208–4219.
(22) Kocabas, C.; Pimparkar, N.; Yesilyurt, O.; Kang, S. J.; Alam, M. A.; Rogers, J. A. *Nano Lett.* **2007**, *7* (5), 1195–1202.
(23) Reese, C.; Roberts, M. E.; Parkin, S. R.; Bao, Z. A. *Appl. Phys. Lett.* **2009**, *94*, 202101.
(24) Sary, N.; Mezzenga, R.; Brochon, C.; Hadziioannou, G.; Ruokolainen, J. *Macromolecules* **2007**, *40* (9), 3277–3286.
(25) Tao, Y. F.; Zohar, H.; Olsen, B. D.; Segalman, R. A. *Nano Lett.* **2007**, *7* (9), 2742–2746.
(26) Olsen, B. D.; Segalman, R. A. *Macromolecules* **2006**, *39* (20), 7078–7083.
(27) Olsen, B. D.; Segalman, R. A. *Macromolecules* **2007**, *40* (19), 6922–6929.
(28) Pryamitsyn, V.; Ganesan, V. *J. Chem. Phys.* **2004**, *120* (12), 5824–5838.
(29) Olsen, B. D.; Alcazar, D.; Krikorian, V.; Toney, M. F.; Thomas, E. L.; Segalman, R. A. *Macromolecules* **2008**, *41* (1), 58–66.
(30) Tao, Y. F.; Olsen, B. D.; Ganesan, V.; Segalman, R. A. *Macromolecules* **2007**, *40* (9), 3320–3327.
(31) Semenov, A. N. *Mol. Cryst. Liq. Cryst.* **1991**, *209*, 191–199.
(32) Matsen, M. W.; Barrett, C. *J. Chem. Phys.* **1998**, *109* (10), 4108–4118.
(33) Olsen, B. D.; Jang, S. Y.; Luning, J. M.; Segalman, R. A. *Macromolecules* **2006**, *39* (13), 4469–4479.
(34) Matsuyama, A. *Phys. Rev. E* **2003**, *67*, 4.
(35) Kempe, M. D.; Kornfield, J. A.; Lal, J. *Macromolecules* **2004**, *37* (23), 8730–8738.